RSC Advances

PAPER

View Article Online
View Journal | View Issue

Open Access Article. Published on 26 April 2024. Downloaded on 3/15/2026 5:27:25 PM.
This article is licensed under a Creative Commons Attribution-NonCommercial 3.0 Unported Licence.

Check for updates

Cite this: *RSC Adv.*, 2024, **14**, 13905

The crucial role of hydrogen bonding in shaping the structures of zinc-based coordination polymers using tridentate N, N, O donor reduced Schiff base ligands and bridging acetates†

Puspendu Middya,[a] Antonio Frontera[b] and Shouvik Chattopadhyay *[a]

Received 22nd January 2024
Accepted 23rd April 2024

DOI: 10.1039/d4ra00550c

rsc.li/rsc-advances

In this manuscript we report the synthesis and characterization of two new polynuclear zinc(II) complexes, $[Zn_2L^1(\mu\text{-}OAc)_3]_n\cdot H_2O$ (**1**) and $[Zn_2L^2(\mu\text{-}OAc)_3]_n$ (**2**) using two tridentate ligands, HL^1 {4-chloro-2-(((2-(methylamino)ethyl)amino)methyl)phenol} and HL^2 {2,4-dibromo-6-(((3-(methylamino)propyl)amino)methyl)phenol}. The structures were confirmed by single-crystal X-ray diffraction analysis. Both complexes form 1D chains. The energy of H-bonding interaction in the solid state structures of the complexes has been estimated by DFT calculation and the crucial role of hydrogen bonding in shaping their structures has been highlighted.

Introduction

Schiff base ligands, characterized by imine bonds, are of interest to inorganic chemists for their wide ranging complexing ability and stability under various oxidative and reductive conditions. Their structural versatility is associated with their diverse applications since long.[1–6] They have been used to prepare numerous transition and non-transition metal complexes, many of which have interesting applications in materials science.[7–11] Many such complexes found application in biochemistry,[12] catalysis,[13] medical imaging,[14] non-linear optics,[15,16] and opto-electronics.[17,18] The application of these complexes in magetochemistry is also noteworthy.[19–23] Among various Schiff bases, salen type N_2O_2 donor ligands, prepared by the 1 : 2 condensation of ethylenediamine and salicylaldehyde, are probably most popular.[24–32] Use of *N*-substituted diamine may produce tridentate N_2O donor Schiff bases and may also be used for forming varieties of complexes.[33–38] These ligands could be reduced with mild reducing agents (*e.g.* sodium borohydride) to form more flexible 'reduced Schiff bases', which may form complexes with various transition and non-transition metals, which have also been shown to have different interesting applications in catalysis, sending and magnetism.[39–44]

Formation of different supramolecular assemblies in the solid state structures of different transition and non-transition metal complexes may be tactfully controlled by exploiting various non-covalent interactions.[45–47] The application of these supramolecular structures in host–guest chemistry, in sensing, and in catalysis is well documented in literature.[48–50] Therefore, a good command over several branches of supramolecular chemistry may be achieved by the systematic study of these non-covalent interactions. The most frequently used methodology to design supramolecular structure in complexes is to employ hydrogen bonds.[51–53] A hydrogen bond is nothing but an interaction of two electronegative atoms with an H atom. The energy of interaction associated with the formation of a hydrogen bond falls approximately in range of 0.25–40 kcal mol^{-1}.[54] It is well known since its discovery that the increasing electronegativity of the interacting atoms increases the energy of H-bonding interaction.[55] Owing to the directional nature and strength hydrogen bonding interaction, crystal engineers frequently used it for the association of discrete molecules into well-organized supramolecules.[56–70]

In the present work, two structurally similar reduced Schiff base ligands have been synthesized and used to form zinc(II) complexes. Supramolecular interactions in the solid state structures of both complexes were studied energetically using theoretical DFT calculations to understand clearly the importance of hydrogen bonding in shaping the structures. These interactions have also been analyzed using several computational tools, including Bader's "atoms-inmolecules" (AIM).

Experimental

All starting materials and solvents were commercially available, reagent grade, and used as purchased from Sigma-Aldrich without further purification.

[a]*Department of Chemistry, Jadavpur University, Kolkata 700032, India. E-mail: shouvik.chattopadhyay@jadavpuruniversity.in*

[b]*Department of Chemistry, Universitat de les Illes Balears, Crta de Valldemossa km 7.5, 07122 Palma de Mallorca (Baleares), Spain. E-mail: toni.frontera@uib.es*

† Electronic supplementary information (ESI) available: Fig. S1–S7 and Table S1–S4. CCDC 2323492 and 2323493 for complexes 1 and 2 respectively. For ESI and crystallographic data in CIF or other electronic format see DOI: https://doi.org/10.1039/d4ra00550c

© 2024 The Author(s). Published by the Royal Society of Chemistry

Open Access Article. Published on 26 April 2024. Downloaded on 3/15/2026 5:27:25 PM. This article is licensed under a Creative Commons Attribution-NonCommercial 3.0 Unported Licence.

Synthesis of the ligands

The ligands have been prepared following the literature methods[71,72] and therefore the synthesis of the ligands is briefly given in the ESI.†

Synthesis of complexes

$[Zn_2L^1(\mu\text{-OAc})_3]_n\cdot H_2O$ (1). A methanol solution (5 mL) of ~2 mmol zinc(II) acetate dihydrate (439 mg) was added to a methanol solution (10 mL) of the reduced 'Schiff base' ligand HL^1 (~1 mmol) with constant stirring. Colourless crystals of the complex **1** were obtained after ten days of slow evaporation in an open atmosphere.

Yield: 435.44 mg (~81%) based on zinc. Anal. Calc. for $C_{16}H_{23}ClN_2O_8Zn_2$ (FW: 537.59): C, 35.75; H, 4.31; N, 5.21. Found: C, 35.72; H, 4.33; N, 5.24%, FT-IR (KBr, cm^{-1}): 3304–3241 (ν_{N-H}), 2924–2864 (ν_{C-H}), 1607–1567 (ν_{COO^-}), 1434–1390 (ν_{COO^-}). UV-vis, λ_{max} (nm), [ε_{max} (L mol^{-1} cm^{-1})] (acetonitrile): 292 (2.817×10^3).

$[Zn_2L^2(\mu\text{-OAc})_3]_n$ (2). Complex **2** was synthesized in a similar procedure to that of complex **1**, except that HL^2 was used instead of HL^1.

Yield: 487.63 mg (~74%) based on zinc. Anal. Calc. for $C_{17}H_{24}Br_2N_2O_7Zn_2$ (FW: 658.96): C, 30.99; H, 3.67; N, 4.25. Found: C, 31.10; H, 3.71; N, 4.32%, FT-IR (KBr, cm^{-1}): 3261–3220 (ν_{N-H}), 2960–2863 (ν_{C-H}), 1605–1562 (ν_{COO^-}), 1405 (ν_{COO^-}). UV-vis, λ_{max} (nm), [ε_{max} (L mol^{-1} cm^{-1})] (acetonitrile): 309 (5.18×10^3).

Physical measurement

Elemental analysis (carbon, hydrogen and nitrogen) was performed using a PerkinElmer 240C elemental analyzer. IR spectra in KBr (4500–500 cm^{-1}) were recorded RX-1 FTIR spectrophotometer. Absorption spectra in acetonitrile solvent were recorded on UV-1900i Shimadzu absorbance spectrophotometer. Emission spectra were recorded in acetonitrile solvent on Duetta-1621 fluorescence spectrophotometer.

X-ray crystallography

A 'Bruker D8 QUEST area detector' diffractometer equipped with graphite-monochromated Mo K_α radiation ($\lambda = 0.71073$ Å) has been used to collect (single crystal) XRD data using suitable crystals (of appropriate dimension) of the complexes. Direct method has been used to solve the structures and refinement was done by full-matrix least squares on F^2 using the SHELXL-18/1 package.[73] Non-hydrogen atoms were refined with anisotropic thermal parameters. The hydrogen atoms attached to nitrogen atoms were located by difference Fourier maps and were kept at fixed positions. All other hydrogen atoms were placed in their geometrically idealized positions and constrained to ride on their parent atoms. Multi-scan empirical absorption corrections were applied to the data using the program SADABS.[74] The details of crystallographic data and refinements have been given in Table S1.† Important bond lengths and angles have been listed in Tables S2 and S3, respectively (ESI).†

Theoretical methods

The H-bonding interactions in this study were analyzed using Gaussian-16 software[75] and the PBE0-D3/def2-TZVP level of theory.[76–78] For evaluating these interactions in their solid-state form, we utilized crystallographic coordinates. The Bader's "Atoms in Molecules" theory (QTAIM)[79,80] was employed for examining the hydrogen bonding interactions, utilizing the AIMAll calculation package for these analyses.[81] The hydrogen bonding interaction has been estimated using the potential energy density (V_g) at the BCP and the equation proposed in the literature.[82]

Results and discussion

Synthesis

A methanol solution of *N*-methyl-1,2-diaminoethane or *N*-methyl-1,3-diaminopropane and 5-chlorosalicylaldehyde or 3,5-dibromosalicylaldehyde in 1 : 1 molar ratio were refluxed to produce tridentate N_2O donor Schiff base ligands, following the literature method.[83–90] $NaBH_4$ was then used as a reducing agent to prepare the reduced analogues (HL^1 and HL^2) of the Schiff base ligands.[71,72] These are essentially secondary amines, but may be considered as a 'reduced Schiff base' to highlight the method of its synthesis. HL^1 and HL^2 on reaction with zinc(II) acetate dihydrate in 1 : 2 molar ratio in presence of few drops of methanol to produce the complexes **1** and **2**. Synthetic routes to complexes have been shown in Schemes 1 and 2.

Description of structures

$[Zn_2L^1(\mu\text{-OAc})_3]_n\cdot H_2O$ (1). X-ray crystal structure determination reveals that the complex **1** crystalizes in orthorhombic space group, *Fdd*2 forming a chain structure, as shown in Fig. 1. The asymmetric unit (Fig. 2) of complex **1** contains two different types of zinc(II) centers, distorted octahedral, Zn(1) and distorted tetrahedral, Zn(2) along with a lattice water molecule. Zn(1), is equatorially coordinated by two amine nitrogen atoms, {N(1) and N(2)}, one phenoxo oxygen atom, O(1), of the N_2O reduced Schiff base unit, $(L^1)^-$ and one bridging acetate oxygen atom, O(4), and axially coordinated by two oxygen atoms, O(2) and $O(7)^i$ (i = symmetry transformation = $-1/4 + x$, $1.25 - y$, $-1/4 + z$) of two bridging acetate units. Zn(2), On the other hand is coordinated by one phenoxo oxygen atom, O(1), of the reduced Schiff base unit $(L^1)^-$ and three oxygen atoms, {O(3), O(5) and O(6)} of three bridging acetate units. The most common geometry of any tetra-coordinated complex is either square planar or tetrahedral. The exact geometry could be calculated from the τ_4 index, which is defined as $\tau_4 = \{360-(a + b)\}/141$, where a and b are the two largest ligand–metal–ligand angles in the four coordinate species.[91] For a perfect square planar system, τ_4 index should be equal to 0. Similarly, for a regular tetrahedral geometry, τ_4 index is very close to 1. The τ_4 index of complex **1** is 0.885, which confirms the distorted tetrahedral geometry of Zn(2) center. The two largest ligand–metal–ligand angles are 120.6(2)° [O(6)–Zn(2)–O(3)] and 114.6(2)° [O(5)–Zn(2)–O(3)] around Zn(2) center. The saturated five member chelate ring [Zn(1)–N(1)–C(8)–C(9)–N(2)], represent a half-chair conformation (Fig. 3) with puckering parameters, $q = 0.473(7)$ Å; $\phi = 263.5(6)°$.[92]

 © 2024 The Author(s). Published by the Royal Society of Chemistry

Open Access Article. Published on 26 April 2024. Downloaded on 3/15/2026 5:27:25 PM.
This article is licensed under a Creative Commons Attribution-NonCommercial 3.0 Unported Licence.

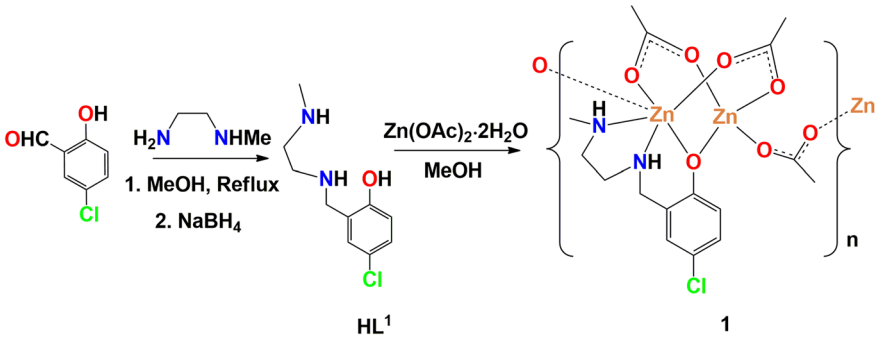

Scheme 1 Synthetic route to complex **1**. Lattice water is not shown for clarity.

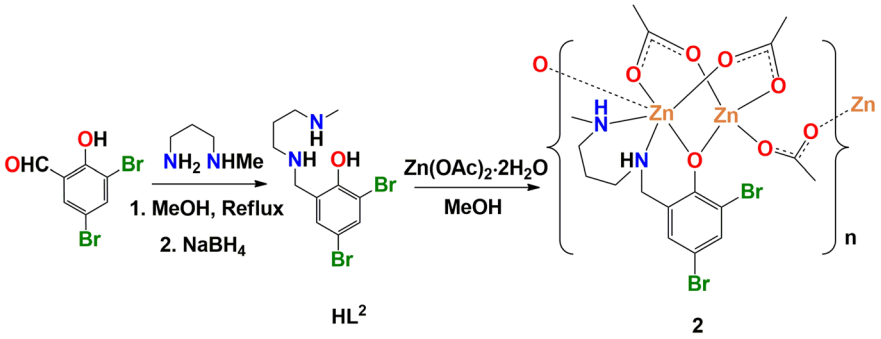

Scheme 2 Synthetic route to complex **2**.

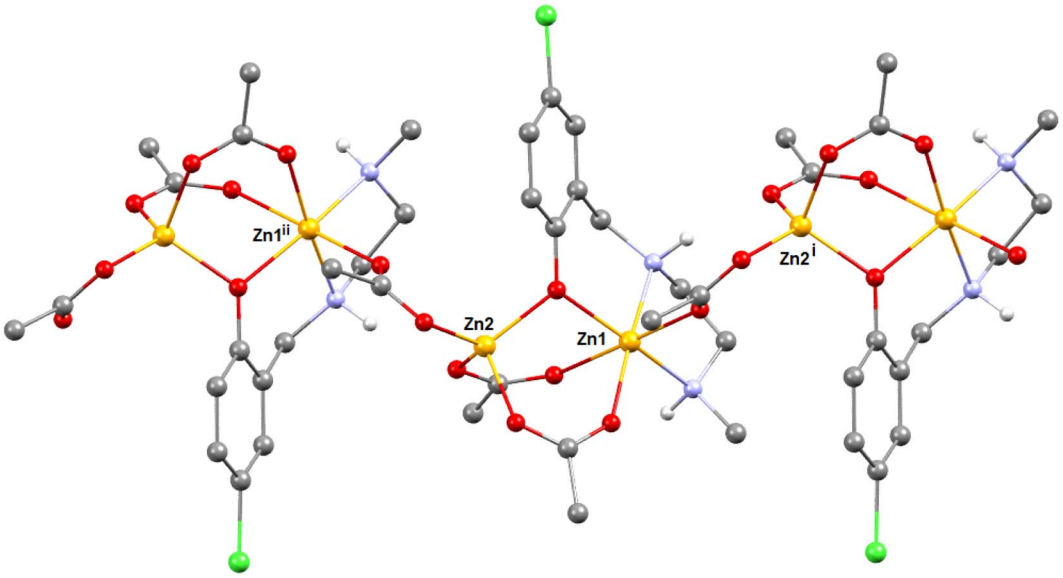

Fig. 1 1D chain of complex **1**. Only amine hydrogen atoms are shown for clarity. Symmetry transformation i = −1/4 + *x*, 1.25 − *y*, −1/4 + *z* and ii = 1/4 + *x*, 1.25 − *y*, 1/4 + *z*. We have maintained a colour codes in this figure: red for oxygen, grey for carbon, light blue for nitrogen, green for chlorine, light grey for hydrogen and orange for zinc centres.

In complex **1**, there are two N–H···O hydrogen bonding interactions involving the lattice water molecule and neighboring monomeric unit. The hydrogen atom, H(1), attached to the amine nitrogen atom, N(1), forms hydrogen bonds (Fig. 4) with the acetate oxygen atom, O(3)^{i} of the neighboring monomeric unit (symmetry transformation i = −1/4 + *x*, 1.25 − *y*, 1/4 + *z*). The hydrogen atom, H(2) attached to the amine nitrogen atom, N(2), of the reduced Schiff base unit, $(L^1)^-$ forms hydrogen bonds (Fig. 4) with the oxygen atom, O(8), of the lattice water molecule. The details of hydrogen bonding interactions are gathered in Table 1.

Open Access Article. Published on 26 April 2024. Downloaded on 3/15/2026 5:27:25 PM.
This article is licensed under a Creative Commons Attribution-NonCommercial 3.0 Unported Licence.

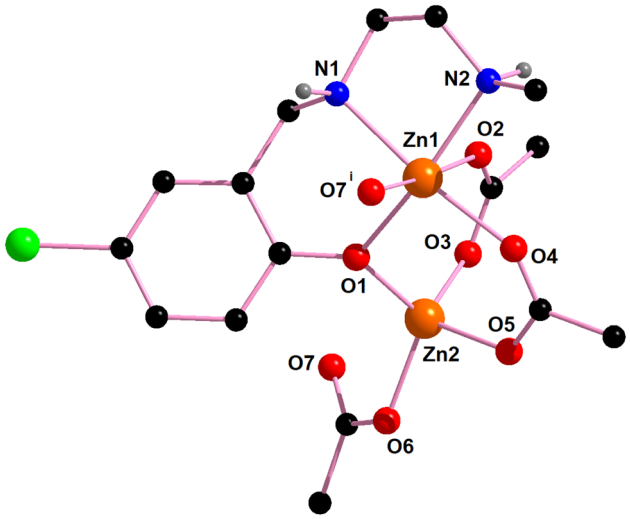

Fig. 2 The asymmetric unit of complex **1**. Lattice water molecule is not shown for clarity. Only the relevant hydrogen atoms are shown for clarity. Symmetry transformation i = −1/4 + *x*, 1.25 − *y*, −1/4 + *z*.

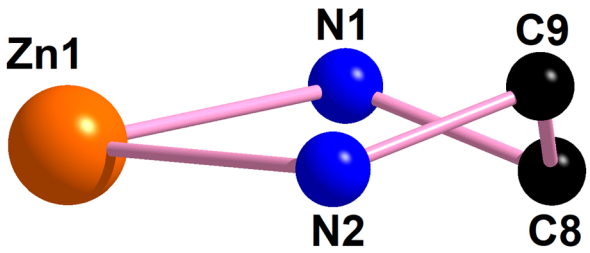

Fig. 3 The perspective view of the half-chair conformation of the saturated five-member chelate ring [Zn(1)–N(1)–C(8)–C(9)–N(2)] of complex **1**.

$[Zn_2L^2(\mu\text{-}OAc)_3]_n$ (2). X-ray crystal structure determination reveals that the complex **2** crystalizes in orthorhombic space group, *Pba*2 forming a chain structure, as shown in Fig. 5. The asymmetric unit (Fig. 6) of complex **2** contains two different types of zinc(II) centers, distorted octahedral, Zn(1) and distorted tetrahedral, Zn(2). Zn(1), is equatorially coordinated by two amine nitrogen atoms, {N(1) and N(2)}, one phenoxo oxygen atom, O(1), of the N_2O reduced Schiff base unit, $(L^2)^-$ and one bridging acetate oxygen atom, O(4), and axially coordinated by two oxygen atoms, {O(2) and O(7)}of two bridging acetate units. Zn(2), On the other hand is coordinated by one phenoxo oxygen atom, O(1), of the reduced Schiff base unit $(L^2)^-$ and three oxygen atoms, {O(3), O(5) and O(6)} of three bridging acetate units. The τ_4 index of the complex **2** is 0.928, which confirms the distorted tetrahedral that the geometry of Zn(2) center. The two largest ligand–metal–ligand angles are 120.1(3)° [O(6)–Zn(2)–O(5)] and 109.1(4)° [O(5)–Zn(2)–O(3)] around Zn(2) center. The saturated six member chelate ring [Zn(1)–N(1)–C(8)–C(9)–C(10)–N(2)], represent a chair conformation (Fig. 7) with puckering parameters, $q = 0.599(14)$ Å; $\theta = 171.5(12)°$; $\phi = 341(9)°$.[92,93]

In complex **2**, additionally, two N–H···O hydrogen bonding interaction exist between the adjacent monomeric units. The hydrogen atoms, H(1) and H(2), attached to the amine nitrogen atoms, N(1) and N(2) of the reduced Schiff base unit, $(L^2)^-$ forms hydrogen bonds (Fig. 8) with the acetate oxygen atoms, $O(5)^{iii}$ and $O(3)^{iii}$ of the neighbouring monomeric unit (symmetry transformation = ^{iii} = −1/4 + *x*, 1.25 − *y*, 1/4 + *z*). The details of hydrogen bonding interactions are gathered in Table 1.

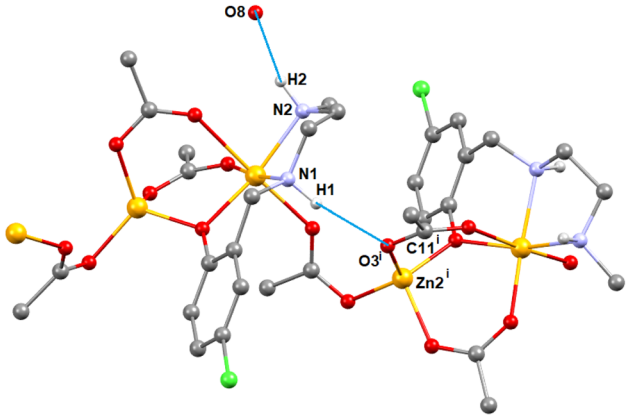

Fig. 4 The N–H···O hydrogen bonding interactions in complex **1**. Only the relevant hydrogen atoms are shown for clarity. Symmetry transformation i = −1/4 + *x*, 1.25 − *y*, −1/4 + *z*. We have maintained a colour codes in this Fig.: red for oxygen, grey for carbon, light blue for nitrogen, green for chlorine, light grey for hydrogen and orange for zinc centres.

Theoretical study

Two novel coordination polymers based on Zn(II) have been successfully synthesized, as depicted in Fig. 9. These complexes can be described as dinuclear Zn(II) motifs with the formula $[Zn_2L^n(AcO)_3]$, connected by bridging acetate ligands. In the case of complex **1**, which includes a lattice water molecule within its composition, the NH amino groups of the reduced Schiff base ligand exhibit divergent orientations (as indicated by the yellow circle). One NH group points towards the water molecule, while the other NH group interacts with the oxygen atom of an acetate group from an adjacent $[Zn_2L^n(AcO)_3]$ unit.

In contrast, complex **2** displays a different arrangement, with both NH groups oriented in the same direction. These NH groups form hydrogen bonds with the acetate ligands of neighboring units. Consequently, NH···OAc hydrogen bonds play a significant role in both the formation and stabilization of the coordination polymers.

Theoretical Density Functional Theory (DFT) analysis is employed to assess the strength of these hydrogen bonds and to investigate the profound impact of the lattice water molecule on the orientation of the NH groups. This, in turn, influences the geometry and arrangement of the polymeric chain.

We conducted QTAIM (Quantum Theory of Atoms in Molecules) analysis on a dimeric fragment of the polymers, represented as tetranuclear models, to assess the strength of the hydrogen bonds. Given the polymeric nature of the structures, the hydrogen bonds were evaluated using the potential energy density at the bond critical points (CPs), as described in the

 © 2024 The Author(s). Published by the Royal Society of Chemistry

Open Access Article. Published on 26 April 2024. Downloaded on 3/15/2026 5:27:25 PM.
This article is licensed under a Creative Commons Attribution-NonCommercial 3.0 Unported Licence.

Table 1 Hydrogen bond distances and angles in complexes **1**–**2**

Complex	N–H···O	N–H (Å)	H···O (Å)	N–H···O (Å)	∠N–H··· O (°)	Symmetry transformation
1	N(1)–H(1)···O(3)^{i}	0.980	2.183	3.153(7)	170.2	i = −1/4 + *x*, 1.25 − *y*, −1/4 + *z*
	N(2)–H(2)···O(8)	0.981	2.117	3.04(1)	155.3	—
2	N(1)–H(1)···O(5)^{iii}	0.980	2.070	3.03(1)	166.7	^{iii} = −0.5 + *x*, 1.5 − *y*, *z*
	N(2)–H(2)···O(3)^{iii}	0.980	2.312	3.26(1)	162.7	

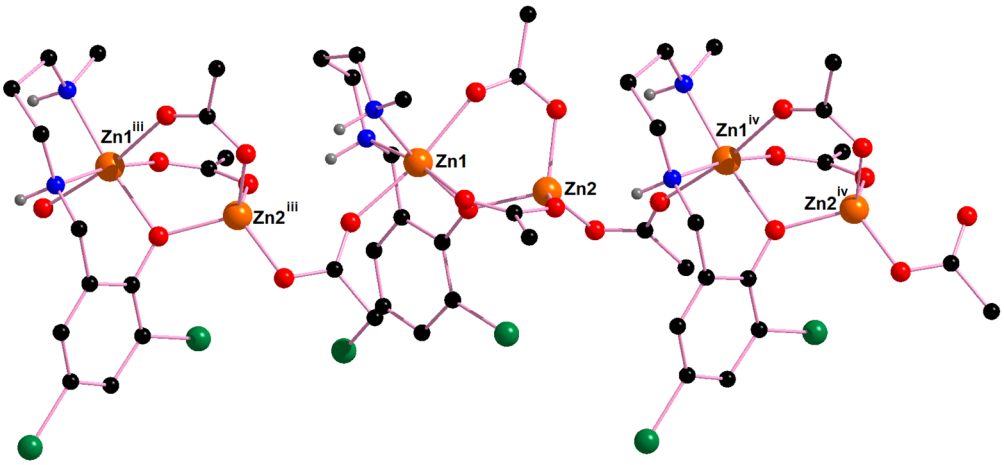

Fig. 5 1D chain of the complex **2**. Only amine hydrogen atoms are shown for clarity. Symmetry transformation iii = −0.5 + *x*, 1.5 − *y*, *z* and iv = 0.5 + *x*, 1.5 − *y*, *z*. We have maintained a colour codes in this figure: red for oxygen, black for carbon, blue for nitrogen, deep green for bromine, grey for hydrogen and orange for zinc centres.

theoretical methods. The QTAIM analysis confirms the presence of NH···OH_2 and NH···OAc hydrogen bonds, which is evident from the existence of corresponding bond critical points (BCP) represented as purple spheres in Fig. 10, as well as bond paths (depicted as dashed bonds) connecting the hydrogen atoms to the oxygen atoms.

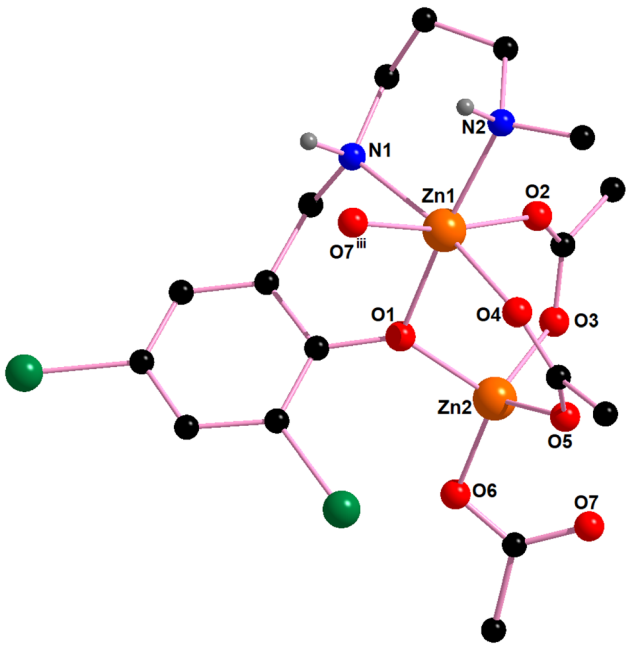

Fig. 6 The asymmetric unit of complex **2**. Only the relevant hydrogen atoms are shown for clarity. Symmetry transformation iii = −0.5 + *x*, 1.5 − *y*, *z*.

It is worth noting that in complex **2**, where no water is present in the solid-state structure, the energy associated with both hydrogen bonds is −6.1 kcal mol^{-1}. However, in complex **1**, the cumulative energy of both hydrogen bonds is slightly more negative, measuring −6.6 kcal mol^{-1}. This difference, albeit small (0.5 kcal mol^{-1}), has a significant cumulative effect along the infinite polymeric chain. Consequently, it explains the distinct arrangement of the NH groups in these complexes.

Therefore, the pronounced influence of the lattice water molecule on the conformation of the polymeric chain can be attributed to the fact that the combination of NH···OAc and NH···OH_2 hydrogen bonds is energetically stronger than the presence of two NH···OAc hydrogen bonds alone.

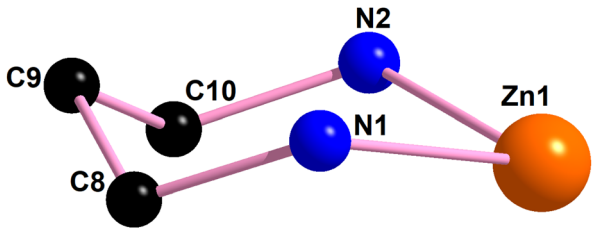

Fig. 7 The perspective view of the chair conformation of the saturated six member chelate ring [Zn(1)–N(1)–C(8)–C(9)–C(10)–N(2)] of complex **2**.

Open Access Article. Published on 26 April 2024. Downloaded on 3/15/2026 5:27:25 PM.
This article is licensed under a Creative Commons Attribution-NonCommercial 3.0 Unported Licence.

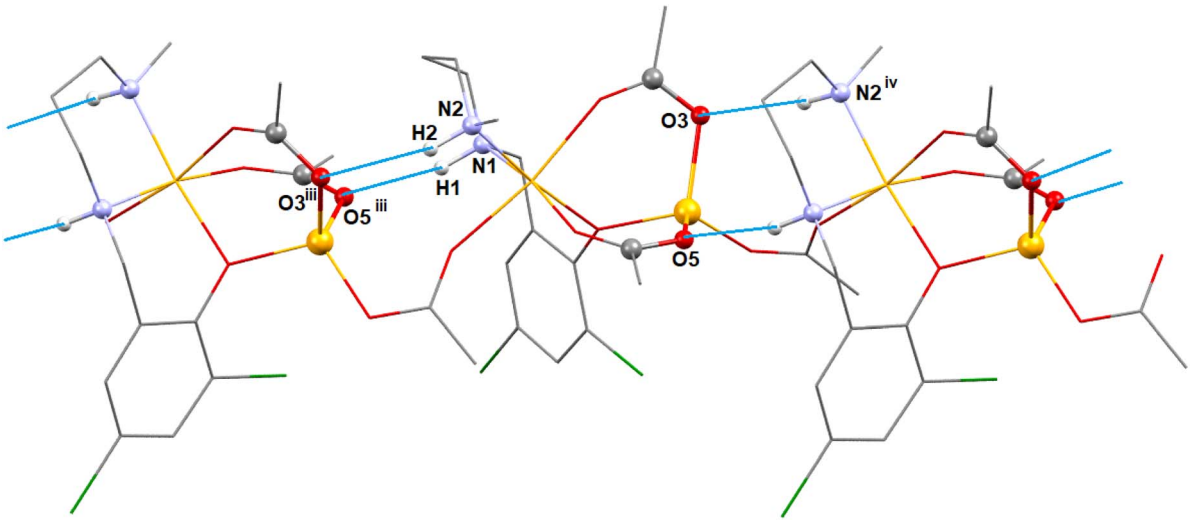

Fig. 8 The N–H···O hydrogen bonding interactions in complex **2**. Only the relevant hydrogen atoms are shown for clarity.

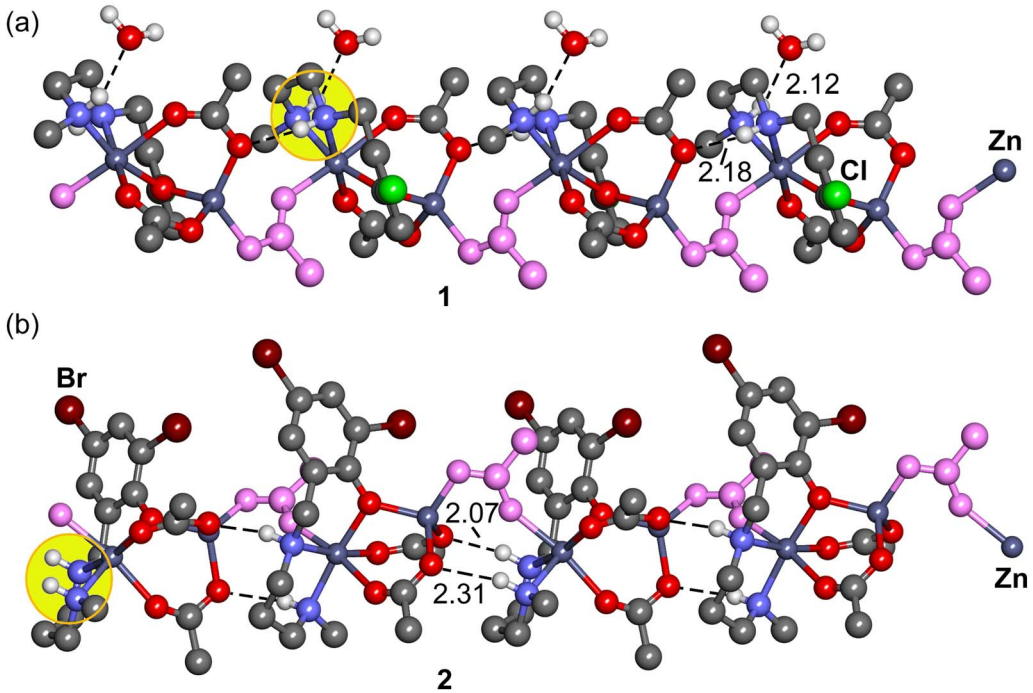

Fig. 9 Representation of the 1D coordination polymers 1 (a) and 2 (b) with indication of the H-bonds. The H-bonded are omitted apart from those participating in the H-bonds. The distances are given in A.

Hirshfeld surface analysis

Fig. S1 and S2 (ESI)† display the Hirshfeld surfaces of complexes **1** and **2**, which are mapped over dnorm, curvedness, and shape index (range −0.1 Å to 1.5 Å). To enable visibility of the molecular moiety around which they are calculated, the surface is rendered as transparent. The dominant interactions are Br···H/H···Br and O···H/H···O of complex **2** can be seen in the Hirshfeld surface as red spots on the d_{norm} surface in Fig. S1.† Other visible spots in the Hirshfeld surfaces corresponds to H···H contacts. The small extent of area and light colour on the surface indicate weaker and longer contact other than hydrogen bonds. C···H/H···C interaction appear as distinct spikes in the 2D fingering plot (Fig. 11). Complementary regions are visible in the fingerprint plots where one molecule acts as a donar ($d_e > d_i$) and the other as an acceptor ($d_e < d_i$). The fingerprint plots can be decomposed to high-light contributions from different interactions types, which overlap in the full fingerprint.[94]

The proportions Br···H/H···Br, O···H/H···O and C···H/H···C, comprises 21.1, 17.2 and 5.7% of the Hirshfeld surface of the complex **2**. Br···H/H···Br interaction appears as two distinct

 © 2024 The Author(s). Published by the Royal Society of Chemistry

Open Access Article. Published on 26 April 2024. Downloaded on 3/15/2026 5:27:25 PM.
This article is licensed under a Creative Commons Attribution-NonCommercial 3.0 Unported Licence.

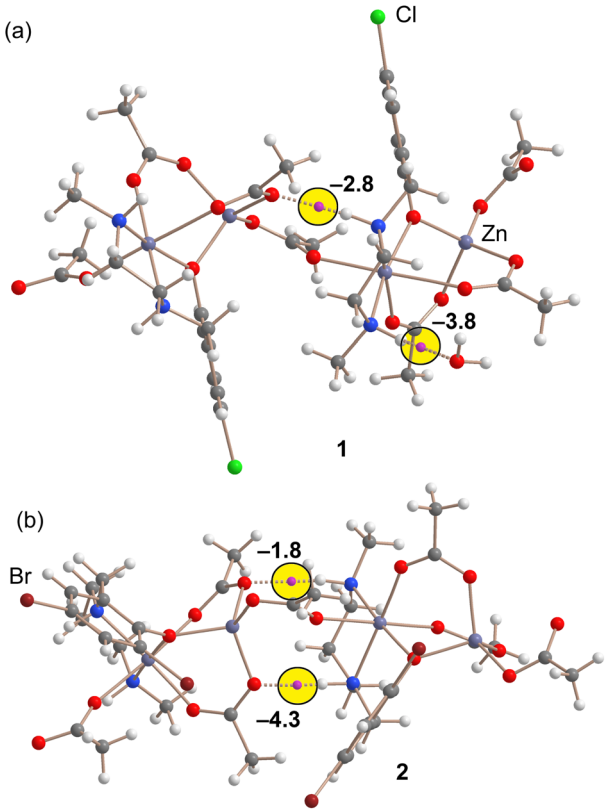

Fig. 10 QTAIM analysis of dimeric models of complexes **1** (a) and **2** (b). Only BCPs (purple spheres) and bond paths (dashed bonds) corresponding to the NH···O H-bonds are represented for clarity. The H-bonding energies are indicated close to the BCPs. We have maintained a colour codes in this figure: red for oxygen, grey for carbon and zinc, blue for nitrogen, green for chlorine, purple for bromine and light grey for hydrogen atoms.

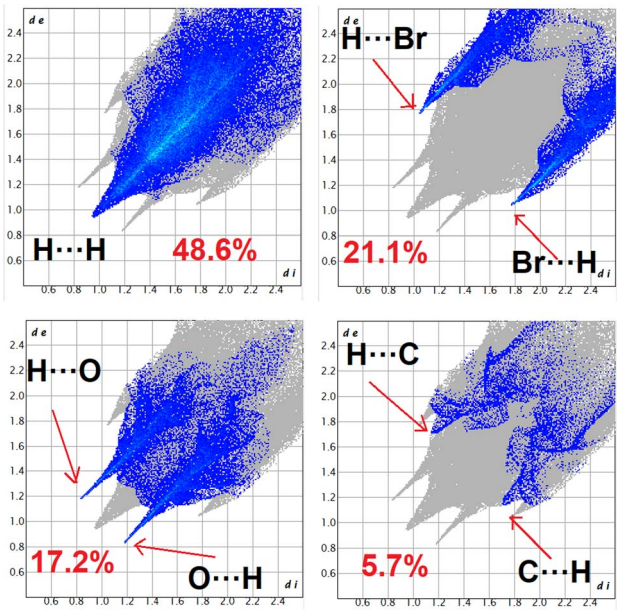

Fig. 11 Fingerprint plot: different contacts contributed to the total Hirshfeld surface area of complex **2**.

spike in the 2D fingerprint plots. The Br···H interaction is represented by lower spike (d_i = 1.78 and d_e = 1.03 Å) and the H···Br interaction is represented by the upper spike (d_i = 1.03 and d_e = 1.78 Å), which can be viewed as bright red spots on the d_{norm} surface. The O···H interaction is represented by lower spike (d_i = 1.18 and d_e = 0.83 Å) and the H···O interaction is represented by upper spike (d_i = 0.83 and d_e = 1.18 Å), which can be viewed as bright red spots on the d_{norm} surface. The C···H interaction is represented by lower spike (d_i = 1.70 and d_e = 1.15 Å) and the H···C interaction is represented by upper spike (d_i = 1.15 and d_e = 1.70 Å), which can be viewed as bright red spots on the d_{norm} surface.

IR spectral study

In the IR spectra of complexes **1** and **2**, distinct bands in the region 3304–3152 are observed due to the presence of N–H stretching vibrations.[95–97] Bands in the region 2924–2863 cm^{-1} may be assigned as C–H stretching vibrations.[53,98,99] The details of the IR bands are gathered in Table S4 (ESI).†

Potential application of the complexes

The complexes may have applications in different fields. Some important potential applications of the complexes are outlined below. Many zinc complexes have been used as photo-catalyst to degrade several oreganic dyes, *e.g.* methylene blue.[100,101] The present complexes may therefore have the potential to be used in the photo-catalytic degradation of different organic dyes and may therefore be used in textile industry for waste management. Literature shows that zinc complexes may mimic several hydrolytic enzymes *e.g.* phosphatase *etc.*[42,102,103] Therefore, the present complexes may have interesting bio-mimetic catalytic application. Many group 12 metal complexes with similar ligands have been utilised to fabricate different opto-electronic devices, some of which have been found to show photo-sensitivity.[17,104] It will therefore be interesting to explore the possibility of fabricating different opto-electronic devices using complexes **1** and **2**. The strong fluorescence emission of many zinc complexes have been exploited for the detection of nitro-aromatic explosives by turn off fluorescence responses.[39,105–107] The present complexes may also be used as sensor to detect different nitroaromatic explosives.

Conclusions

In summary, we have synthesized two zinc complexes. Both are forming 1D chains. We have estimated the energy of H-bonding interaction in the solid state structures of the complexes. Our analysis highlights the crucial role of hydrogen bonding in shaping the structures of Zn(II)-based coordination polymers. Complex **1**, with a lattice water molecule, shows slightly stronger combined hydrogen bond energy than complex **2**, lacking water. This modest energy difference significantly influences the orientation of NH groups and the polymer's arrangement. Although the application of the complexes were not explored in the present study, a literature survey on zinc complexes with similar Schiff bases or their reduced analogues

Open Access Article. Published on 26 April 2024. Downloaded on 3/15/2026 5:27:25 PM. This article is licensed under a Creative Commons Attribution-NonCommercial 3.0 Unported Licence.

indicates that the complexes may have the potential application in detecting nitroarmatic explosives, in the fabrication of opto-electronic devices, in the photo-catalytic degradation of organic dyes and also in mimicking different hydrolytic enzymes *etc.*

Conflicts of interest

There are no conflicts to declare.

Acknowledgements

P. Middya thanks the UGC, India, for awarding a Senior Research Fellowship (NFSC). This research was funded by MICIU/AEI of Spain (project PID2020-115637GB-I00 FEDER funds). We thank the "centre de technologies de la informació" (CTI) at the University of the Balearic Islands for computational facilities.

Notes and references

1 R. Ziessel, *Coord. Chem. Rev.*, 2001, **216**, 195.
2 P. G. Cozzi, *Chem. Soc. Rev.*, 2004, **33**, 410.
3 K. C. Gupta and A. K. Sutar, *Coord. Chem. Rev.*, 2008, **252**, 1420.
4 J. P. Costes, S. Shova and W. Wernsdorfer, *Dalton Trans.*, 2008, 1843.
5 X. G. Ran, L. Y. Wang, Y. C. Lin, J. Hao and D. R. Cao, *Appl. Organomet. Chem.*, 2010, **24**, 741.
6 M. Orio, O. Jarjayes, H. Kanso, C. Philouze, F. Neese and F. Thomas, *Angew. Chem., Int. Ed.*, 2010, **49**, 4989.
7 X. Liu and J.-R. Hamon, *Coord. Chem. Rev.*, 2019, **389**, 94–118.
8 N. Cao, R. Jiang, L. Hao, L. Tian, R. Moc, Y. Fan, J. Zhao and L. Ren, *Mater. Lett.*, 2019, **250**, 182–185.
9 S.-H. Lee, S.-R. Shin and D.-S. Lee, *Mater. Des.*, 2019, **172**, 107774.
10 A. Panja and K. Ghosh, *Mater. Chem. Front.*, 2018, **2**, 1866–1875.
11 S. Kr. Saha and P. Banerjee, *Mater. Chem. Front.*, 2018, **2**, 1674–1691.
12 N. Ahmed, C. Das, S. Vaidya, A. K. Srivastava, S. K. Langley, K. S. Murray and M. Shanmugam, *Dalton Trans.*, 2014, **43**, 17375–17384.
13 X. Yang, D. Schipper, R. A. Jones, L. A. Lytwak, B. J. Holliday and S. Huang, *J. Am. Chem. Soc.*, 2013, **135**, 8468–8471.
14 S. Sarkar and K. A. Dey, *Spectrochim. Acta, Part A*, 2010, **77**, 740–748.
15 A. Kösea, Ö. Güngör, J. N. Ballı and S. Erkan, *J. Mol. Struct.*, 2022, **1268**, 133750.
16 S. Celedón, T. Roisnel, V. Artigas, M. Fuentealba, D. Carrillo, I. Ledoux-Rak, J.-R. Hamon and C. Manzur, *New J. Chem.*, 2020, **44**, 9190–9201.
17 S. Roy, A. Dey, P. P. Ray, J. Ortega-Castro, A. Frontera and S. Chattopadhyay, *Chem. Commun.*, 2015, **51**, 12974–12976.
18 S. Khan, S. Halder, P. P. Ray, S. Herrero, R. González-Prieto, M. G. B. Drew and S. Chattopadhyay, *Cryst. Growth Des.*, 2018, **18**, 651–659.
19 P. Bhowmik, H. P. Nayek, M. Corbella, N. Aliaga-Alcalde and S. Chattopadhyay, *Dalton Trans.*, 2011, **40**, 7916–7926.
20 S. Naiya, S. Biswas, M. G. B. Drew, C. J. Gómez-García and A. Ghosh, *Inorg. Chem.*, 2012, **51**, 5332–5341.
21 P. Kar, P. M. Guha, M. G. B. Drew, T. Ishida and A. Ghosh, *Eur. J. Inorg. Chem.*, 2011, 2075–2085.
22 B. Sarkar, M. S. Ray, Y.-Z. Li, Y. Song, A. Figuerola, E. Ruiz, J. Cirera, J. Cano and A. Ghosh, *Chem.–Eur. J.*, 2007, **13**, 9297–9309.
23 S. Chattopadhyay, M. G. B. Drew, C. Diaz and A. Ghosh, *Dalton Trans.*, 2007, 2492–2494.
24 S. Shaw and J. D. White, *Chem. Rev.*, 2019, **119**, 9381–9426.
25 B. Agrahari, S. Layek, R. Ganguly and D. D. Pathak, *New J. Chem.*, 2018, **42**, 13754–13762.
26 A. Finelli, N. Hérault, A. Crochet and K. M. Fromm, *Cryst. Growth Des.*, 2018, **18**, 1215–1226.
27 S. I. Samponi, V. Zdorichenko, M. Danopoulou, M. C. Leech, K. Lam, A. Abdul-Sada, B. Cox, G. J. Tizzard, S. J. Coles, A. Tsipis and G. E. Kostakis, *Dalton Trans.*, 2020, **49**, 289–299.
28 A. Singh, A. Maji, A. Mohanty and K. Ghosh, *New J. Chem.*, 2020, **44**, 18399–18418.
29 A. Bhunia, P. W. Roesky, Y. Lan, G. E. Kostakis and A. K. Powell, *Inorg. Chem.*, 2009, **48**, 10483–10485.
30 N. Mahlooji, M. Behzad, H. A. Rudbari, G. Bruno and B. Ghanbari, *Inorg. Chim. Acta*, 2016, **445**, 124–128.
31 L. S. Felices, E. C. Escudero-Adán, J. Benet-Buchholz and A. W. Kleij, *Inorg. Chem.*, 2009, **48**, 846–853.
32 P. Asadollahi, R. Bikas, M. S. Krawczyk and T. Lis, *Polyhedron*, 2022, **211**, 115537.
33 S. Roy, T. Dutta, M. G. B. Drew and S. Chattopadhyay, *Polyhedron*, 2020, **178**, 114311.
34 P. Liu, X.-J. Feng and R. He, *Tetrahedron*, 2010, **66**, 631–636.
35 M. J. Romero, R. Pedrido, A. M. González-Noya, M. Maneiro, M. I. Fernandez-García, G. Zaragoza and M. R. Bermejo, *Dalton Trans.*, 2012, **41**, 10832–10844.
36 L. Rigamonti, A. Forni, M. Sironi, A. Ponti, A. M. Ferretti, C. Baschieri and A. Pasini, *Polyhedron*, 2018, **145**, 22–34.
37 P. Bhowmik, S. Jana, P. Mahapatra, S. Giri, S. Chattopadhyay and A. Ghosh, *Polyhedron*, 2018, **145**, 43–52.
38 P. Pandey, A. Verma, K. Bretosh, J.-P. Sutter and S. S. Sunkari, *Polyhedron*, 2019, **164**, 80–89.
39 M. Karmakar, S. Roy and S. Chattopadhyay, *New J. Chem.*, 2019, **43**, 10093–10102.
40 A. Biswas, M. G. B. Drew, C. J. Gomez-Garcia and A. Ghosh, *Inorg. Chem.*, 2010, **49**, 8155–8163.
41 A. Biswas, L. K. Das, M. G. B. Drew, C. Diaz and A. Ghosh, *Inorg. Chem.*, 2012, **51**, 10111–10121.
42 M. Karmakar, T. Basak and S. Chattopadhyay, *New J. Chem.*, 2019, **43**, 4432–4443.
43 C.-T. Yang, M. Vetrichelvan, X. Yang, B. Moubaraki, K. S. Murray and J. J. Vittal, *Dalton Trans.*, 2004, 113–121.
44 A. Banerjee, S. Banerjee, C. J. Gomez Garc, S. Benmansour and S. Chattopadhyay, *ACS Omega*, 2019, **4**, 20634–20643.

 © 2024 The Author(s). Published by the Royal Society of Chemistry

Open Access Article. Published on 26 April 2024. Downloaded on 3/15/2026 5:27:25 PM.
This article is licensed under a Creative Commons Attribution-NonCommercial 3.0 Unported Licence.

45 G. Consiglio, S. Failla, P. Finocchiaro, I. P. Oliveri, R. Purrello and S. D. Bella, *Inorg. Chem.*, 2010, **49**, 5134–5142.
46 S. Banerjee, P.-G. Lassahn, C. Janiak and A. Ghosh, *Polyhedron*, 2005, **24**, 2963–2971.
47 P. J. Stang and B. Olenyuk, *Acc. Chem. Res.*, 1997, **30**, 502–518.
48 S. Horiuchi, R. Kumai and Y. Tokura, *J. Am. Chem. Soc.*, 2005, **127**, 5010–5011.
49 S. Roy, M. G. B. Drew, A. Frontera and S. Chattopadhyay, *ChemistrySelect*, 2017, **2**, 7880–7887.
50 M. N. Ahamad, K. Iman, M. K. Raza, M. Kumar, A. Ansari, M. Ahmad and M. Shahid, *Bioorg. Chem.*, 2020, **95**, 103561.
51 P. K. Bhaumik, A. Frontera and S. Chattopadhyay, *Inorg. Chim. Acta*, 2021, **515**, 120023–120030.
52 S. Thakur, M. G. B. Drew, A. Franconetti, A. Frontera and S. Chattopadhyay, *RSC Adv.*, 2019, **9**, 35165–35175.
53 M. Karmakar, A. Frontera and S. Chattopadhyay, *CrystEngComm*, 2021, **23**, 1918–1928.
54 G. R. Desiraju, *Acc. Chem. Res.*, 2002, **35**, 565–573.
55 L. Pauling, *The Nature of the Chemical Bond*, Cornell University Press, Ithaca, New York, 1939.
56 E. Andris, M. Straka, J. Vrána, A. Růžička, J. Roithová and L. Rulíšek, *Chem.–Eur. J.*, 2023, **29**, e202203769.
57 A. W. Schaefer, M. A. Ehudin, D. A. Quist, J. A. Tang, K. D. Karlin and E. I. Solomon, *J. Am. Chem. Soc.*, 2019, **141**, 4936–4951.
58 R. Gaur, S. Roy, P. Kallem and F. Banat, *J. Mol. Struct.*, 2022, **1265**, 133400.
59 M. A. Ehudin, A. W. Schaefer, S. M. Adam, D. A. Quist, D. E. Diaz, J. A. Tang, E. I. Solomon and K. D. Karlin, *Chem. Sci.*, 2019, **10**, 2893–2905.
60 C. Bravo, F. Galego and V. André, *CrystEngComm*, 2019, **21**, 7199–7203.
61 D. Li and K. Kaneko, *Chem. Phys. Lett.*, 2001, **335**, 50–56.
62 J. E. Caton Jr and C. V. Banks, *Inorg. Chem.*, 1967, **9**, 1670–1675.
63 S. D. Kurbah and N. S. Clovis, *Inorg. Chim. Acta*, 2020, **511**, 119837.
64 S. Bosch, P. Comba, L. R. Gahan and G. Schenk, *Inorg. Chem.*, 2014, **53**, 9036–9051.
65 J. C. Mareque-Rivas, R. Prabaharan and R. T. M. de Rosales, *Chem. Commun.*, 2004, 76–77.
66 H. Duan, W. Dan and X. Fang, *J. Solid State Chem.*, 2018, **260**, 159–164.
67 M. Karmakar, W. Sk, R. M. Gomiila, M. G. B. Drew, A. Frontera and S. Chattopadhyay, *RSC Adv.*, 2023, **13**, 21211–21224.
68 M. A. Kinzhalov, D. M. Ivanov, A. V. Shishkina, A. A. Melekhova, V. V. Suslonov, A. Frontera, V. Y. Kukushkin and N. A. Bokach, *Inorg. Chem. Front.*, 2023, **10**, 1522–1533.
69 C. E. MacBeth, R. Gupta, K. R. Mitchell-Koch, V. G. Young Jr, G. H. Lushigtobn, W. H. Thompson, M. P. Hendrich and A. S Borovik, *J. Am. Chem. Soc.*, 2004, **126**, 2556–2567.
70 C. S. Hong, J. H. Yoon and Y. S. You, *Inorg. Chim. Acta*, 2005, **358**, 3341–3346.
71 A. Mondal, A. Sarkar, A. Adhikary, D. Samanta and D. Das, *Dalton Trans.*, 2020, **49**, 15461–15472.
72 J. M. Payne, M. Kamran, M. G. Davidson and M. D. Jones, *ChemSusChem*, 2022, **15**, e202200225.
73 G. M. Sheldrick, *Acta Crystallogr. Sect.*, 2015, **71**, 3–8.
74 G. M. Sheldrick, *SADABS, V2014/5, Software for Empirical Absorption Correction*, University of Göttingen, Gottingen, Germany, 1999.
75 M. J. Frisch, G. W. Trucks, H. B. Schlegel, G. E. Scuseria, M. A. Robb, J. R. Cheeseman, G. Scalmani, V. Barone, G. A. Petersson, H. Nakatsuji, X. Li, M. Caricato, A. V. Marenich, J. Bloino, B. G. Janesko, R. Gomperts, B. Mennucci, H. P. Hratchian, J. V. Ortiz, A. F. Izmaylov, J. L. Sonnenberg, D. Wil-liams-Young, F. Ding, F. Lipparini, F. Egidi, J. Goings, B. Peng, A. Petrone, T. Henderson, D. Ranasinghe, V. G. Zakrzewski, J. Gao, N. Rega, G. Zheng, W. Liang, M. Hada, M. Ehara, K. Toyota, R. Fukuda, J. Hasegawa, M. Ishida, T. Nakajima, Y. Honda, O. Kitao, H. Nakai, T. Vreven, K. Throssell, J. A. Montgomery Jr, J. E. Peralta, F. Ogliaro, M. J. Bearpark, J. J. Heyd, E. N. Brothers, K. N. Kudin, V. N. Staroverov, T. A. Keith, R. Kobayashi, J. Normand, K. Raghavachari, A. P. Rendell, J. C. Burant, S. S. Iyengar, J. Tomasi, M. Cossi, J. M. Millam, M. Klene, C. Adamo, R. Cammi, J. W. Ochterski, R. L. Martin, K. Morokuma, O. Farkas, J. B. Foresman, and D. J. Fox, *Gaussian 16*, Revision C.01, Gaussian, Inc., Wallingford CT, 2016.
76 C. Adamo and V. Barone, *J. Chem. Phys.*, 1999, **110**, 6158–6170.
77 S. Grimme, J. Antony, S. Ehrlich and H. Krieg, *J. Chem. Phys.*, 2010, **132**, 154104–154118.
78 F. Weigend, *Phys. Chem. Chem. Phys.*, 2006, **8**, 1057–1065.
79 R. F. W. Bader, *Chem. Rev.*, 1991, **91**(5), 893–928.
80 R. F. W. Bader, *J. Phys. Chem. A*, 1998, **102**, 7314–7323.
81 T. A. Keith, *TK Gristmill Software*, AIMAll (Version 19.10.12), Overland Park KS, USA, 2019, **https://aim.tkgristmill.com/**.
82 E. Espinosa, E. Molins and C. Lecomte, *Chem. Phys. Lett.*, 1998, **285**, 170–173.
83 A. Banerjee, A. Frontera and S. Chattopadhyay, *Dalton Trans.*, 2019, **48**, 11433–11447.
84 S. Roy, A. Dey, M. G. B. Drew, P. P. Ray and S. Chattopadhyay, *New J. Chem.*, 2019, **43**, 5020–5031.
85 M. Das, S. Chatterjee, K. Harm, T. K. Mondal and S. Chattopadhyay, *Dalton Trans.*, 2014, **43**, 2936–2947.
86 N. Sarkar, M. G. B. Drew, K. Harms, A. Bauza, A. Frontera and S. Chattopadhyay, *CrystEngComm*, 2018, **20**, 1077–1086.
87 A. Bannerjee, D. Das, P. P. Ray, S. Banerjee and S. Chattopadhyay, *Dalton Trans.*, 2021, **50**, 1721.
88 S. Thakur, S. Banerjee, S. Das and S. Chattopadhyay, *New J. Chem.*, 2019, **43**, 18747–18759.
89 S. Khan, S. Sproules, L. S. Natrajan, K. Harms and S. Chattopadhyay, *New J. Chem.*, 2018, **42**, 1634–1641.
90 I. Mondal, T. Basak, S. Banerjee and S. Chattopadhyay, *CrystEngComm*, 2020, **22**, 3005–3019.
91 L. Yang, D. R. Powell and R. P. Houser, *Dalton Trans.*, 2007, 955–964.

Open Access Article. Published on 26 April 2024. Downloaded on 3/15/2026 5:27:25 PM.
This article is licensed under a Creative Commons Attribution-NonCommercial 3.0 Unported Licence.

92 D. Cremer and J. A. Pople, *J. Am. Chem. Soc.*, 1975, **97**, 1354–1358.
93 D. Cremer, *Acta Crystallogr.*, 1984, **40**, 498–500.
94 M. A. Spackman and P. G. Byrom, *Chem. Phys. Lett.*, 1997, **267**, 215–220.
95 S. Chattopadhyay, M. S. Ray, S. Chaudhuri, G. Mukhopadhyay, G. Bocelli, A. Cantoni and A. Ghosh, *Inorg. Chim. Acta*, 2006, **359**, 1367–1375.
96 A. Hazari, R. M. Gomila, A. Frontera, M. G. B. Drew and A. Ghosh, *CrystEngComm*, 2021, **23**, 4848–4856.
97 D. Pellico, M. Gomez-Gallego, R. Escudero, P. Ramirez-Lopez, M. Olivan and M. A. Sierra, *Dalton Trans.*, 2011, **40**, 9145–9153.
98 K. Ghosh, S. Roy, A. Ghosh, A. Banerjee, A. Bauzá, A. Frontera and S. Chattopadhyay, *Polyhedron*, 2006, **112**, 6–17.
99 A. K. Sharma, F. Lloret and R. Mukherjee, *Inorg. Chem.*, 2013, **52**, 4825–4833.
100 T. Basak, A. Bhattacharyya, K. Harms and S. Chattopadhyay, *Polyhedron*, 2019, **157**, 449–457.
101 M. Karmakar and S. Chattopadhyay, *Polyhedron*, 2020, **184**, 114527.
102 T. Basak, M. G. B. Drew and S. Chattopadhyay, *Inorg. Chem. Commun.*, 2018, **98**, 92–98.
103 T. Basak, A. Bhattacharyya, M. Das, K. Harms, A. Bauzá, A. Frontera and S. Chattopadhyay, *ChemistrySelect*, 2017, **2**, 6286–6295.
104 S. Roy, A. Dey, R. M. Gomila, J. Ortega-Castro, A. Frontera, P. P. Ray and S. Chattopadhyay, *Dalton Trans.*, 2022, **51**, 5721–5734.
105 T. Basak, S. Roy, S. Banerjee and S. Chattopadhyay, *Inorg. Chim. Acta*, 2022, **543**, 121186.
106 I. Mondal, S. Chatterjee and S. Chattopadhyay, *Polyhedron*, 2020, **190**, 114735.
107 M. Karmakar and S. Chattopadhyay, *Polyhedron*, 2020, **187**, 114639.

 © 2024 The Author(s). Published by the Royal Society of Chemistry